

Calculating the soft function for thrust: A first look at QFT and SCET

Anna Ferdinand (10453410)

Department of Physics and Astronomy

University of Manchester

November 2022

Abstract

As we enter a new era of precision measurements at the Large Hadron Collider, developing the theoretical tools necessary for accurately describing high energy particle collisions is more important than ever. One framework which has been successful in enabling high precision calculations of observables in such collisions is soft collinear effective theory (SCET). A main element of SCET is its factorization theorems that describe the distinct contributions from low energy (soft) and collinear radiation to observables in certain regimes. In this work we provide an introduction to the use of SCET in precision collider physics by calculating the soft function for thrust, a key component of the thrust factorization theorem, which describes the contribution of soft radiation to the thrust cross-section. To perform this calculation, the basics of quantum field theory (QFT) and Feynman diagrams are outlined to derive the eikonal vertex for a soft emission. After a brief introduction to jets and thrust in SCET, the calculation of the thrust soft function is carried out in the process of which infrared (IR) and ultraviolet (UV) divergences are encountered. The cancellation of the IR divergence is demonstrated, and dimensional regularization is applied to treat the UV divergence. Applications of SCET to current research are discussed, in particular its use in describing observables of jets which have been groomed by the soft drop algorithm.

Word count: 5981

Contents

1	Introduction	3
2	Basics of QFT	3
2.1	Time-dependent perturbation theory	3
2.2	Constructing the scalar field	5
2.3	Including charge	6
2.4	Massless spin-1 fields	7
3	Feynman diagrams	7
3.1	Evaluating an S-matrix element	7
3.2	Diagrammatic representation	8
3.3	The eikonal vertex	9
4	Thrust in SCET	10
4.1	Dijet production and thrust	10
4.2	Factorization theorem for thrust	11
4.3	SCET Feynman diagrams	12
5	Calculating the soft function for thrust	13
5.1	Setting up the calculation	13
5.2	Real contribution	14
5.3	Virtual contribution	16
5.4	Combining the pieces	17
6	Factorization and soft functions in current research	17
7	Summary	18
A	Supplements for soft function calculation	20
A.1	Real contribution in 4 dimensions	20
A.2	Real contribution in d dimensions	21
A.3	Virtual contribution	22

1 Introduction

High energy particle collisions have become the most prominent experimental method for probing new physics and testing current theories. With the Large Hadron Collider (LHC) producing vast amounts of high quality data, the research effort towards making precision measurements of fundamental physical constants is increasingly important. However, the strong interactions that dominate such particle collisions pose a significant theoretical challenge in achieving this goal due to the inherent difficulty of performing calculations in quantum chromodynamics. An exciting new framework which circumvents some of these complications is soft collinear effective theory (SCET) [1]. With a variety of observables receiving enhanced contributions from low energy (soft) and collinear radiation in certain regimes, SCET has found great success in advancing precision collider physics by providing a new framework for understanding the factorization of soft and collinear radiation. By applying SCET, this work seeks to calculate the soft function for the thrust observable which describes the contribution of soft radiation to the thrust cross-section. To carry out this calculation we must begin by becoming acquainted with Feynman diagrams, the basis of which is quantum field theory (QFT) which we outline the foundations of in section 2 before arriving at Feynman diagrams in section 3. Section 4 sets the stage for the calculation of the soft function, discussing jets, thrust, and SCET. We will then be in a position to perform the soft function calculation which we do in section 5. Some applications of soft functions and SCET to current research in precision collider physics are discussed in section 6, followed by a summary in section 7.

2 Basics of QFT

We begin by exploring time-dependent perturbation theory, one of the cornerstones of QFT. By doing so in the framework of quantum mechanics, we will arrive at an intuitive definition of the S-matrix which when required to be Lorentz invariant lays the foundation for the description of particles as fields. The form of these fields for spin-0 and spin-1 particles will be motivated as they are a key component in deriving the Feynman rules relevant for calculating the soft function.

2.1 Time-dependent perturbation theory

Consider a Hamiltonian H_0 with well-known eigenstates labelled $|\alpha\rangle, |\beta\rangle$, and so forth, which is perturbed by a time-dependent perturbation $V(t)$. A useful perspective for investigating this problem is the interaction picture in which H_0 describes the evolution of the observable operators, whereas the interaction picture perturbation operator $V_I(t)$, defined as [2]

$$V_I(t) = e^{\frac{iH_0t}{\hbar}} V(t) e^{-\frac{iH_0t}{\hbar}}, \quad (2.1)$$

describes the evolution of the state kets. The Schrödinger equation in the interaction picture is then given by

$$i\hbar \frac{\partial}{\partial t} |\psi, t_0; t\rangle_I = V_I(t) |\psi, t_0; t\rangle_I, \quad (2.2)$$

where $|\psi, t_0; t\rangle_I$ is a state at time t which at time t_0 was in the state $|\psi, t_0\rangle$ and the subscript I indicates the interaction picture. The solution of Eq. 2.2 can be written in terms of the interaction

picture time-evolution operator $U_I(t, t_0)$

$$|\psi, t_0; t\rangle_I = U_I(t, t_0) |\psi, t_0; t_0\rangle_I . \quad (2.3)$$

This operator has immense physical significance as we can consider $\langle\beta| U_I(t, t_0) |\alpha\rangle$ to be the transition amplitude for going from state $|\alpha\rangle$ at time t_0 to state $|\beta\rangle$ at time t . Combining Eq. 2.2 and Eq. 2.3 with the boundary condition $U_I(t, t_0)|_{t=t_0} = \mathbb{1}$ gives the solution

$$U_I(t, t_0) = \mathbb{1} - \frac{i}{\hbar} \int_{t_0}^t dt' V_I(t') U_I(t', t_0) , \quad (2.4)$$

which we can iterate to obtain the expansion

$$U_I(t, t_0) = 1 - \frac{i}{\hbar} \int_{t_0}^t dt_1 V_I(t_1) - \frac{1}{\hbar^2} \int_{t_0}^t dt_1 \int_{t_0}^{t_1} dt_2 V_I(t_1) V_I(t_2) + \dots , \quad (2.5)$$

known as the Dyson series [2]. This expression for the time-evolution operator finds great use in scattering theory. Consider an experiment in which two sets of particles approach each other, briefly interact, and then move apart. This problem is readily described in the framework of time-dependent perturbation theory. The interaction between the particles may be considered to be a perturbation, only present in the brief window of interaction when the particles are close. As is the case in a usual experimental setup, we take the initial state of the particles at time t_0 to be known and their final state at time t to be unknown. Since any measurement of the final state will be made at a much later time than when the interaction occurred, we are justified in taking the limits $t_0 \rightarrow -\infty$ and $t \rightarrow \infty$. We now define the S-operator as [3]

$$S \equiv U_I(t = \infty, t_0 = -\infty) , \quad (2.6)$$

and the elements of the S-matrix as $S_{\beta\alpha} \equiv \langle\beta| S |\alpha\rangle$ which may, as for $U_I(t, t_0)$, be interpreted as the amplitude of a transition from state $|\alpha\rangle$ to $|\beta\rangle$ in such a scattering experiment. Using the Dyson series in Eq. 2.5, we obtain an explicit form for the S-operator as [3]

$$S = \mathbb{1} + \sum_{n=1}^{\infty} \frac{(-i)^n}{n!} \int_{-\infty}^{\infty} dt_1 dt_2 \dots dt_n \mathcal{T}\{V_I(t_1), V_I(t_2) \dots V_I(t_n)\} , \quad (2.7)$$

now setting $\hbar = 1$ and using the time-ordered product of operators $\mathcal{T}\{V_I(t_1), V_I(t_2) \dots V_I(t_n)\}$ which for two arguments is defined as [3]

$$\mathcal{T}\{V_I(t_1), V_I(t_2)\} = \Theta(t_1 - t_2) V_I(t_1) V_I(t_2) + \Theta(t_2 - t_1) V_I(t_2) V_I(t_1) , \quad (2.8)$$

where Θ is the Heaviside step function, a definition which is easily extended to $n > 2$ arguments. As the S-matrix gives amplitudes for transitions, it is required to be Lorentz invariant as transition probabilities should be independent of frame. Expressing Eq. 2.7 in a manifestly Lorentz invariant form is simple if we hypothesize that the interaction perturbation may be written as [3]

$$V_I(t) = \int d^3x \mathcal{H}(\mathbf{x}, t) , \quad (2.9)$$

where $\mathcal{H}(\mathbf{x}, t)$ is the interaction Hamiltonian density, henceforth just referred to as the Hamiltonian density. This allows us to rewrite Eq. 2.7 as

$$S = \mathbb{1} + \sum_{n=1}^{\infty} \frac{(-i)^n}{n!} \int_{-\infty}^{\infty} d^4x_1 \dots d^4x_n \mathcal{T}\{\mathcal{H}(x_1) \dots \mathcal{H}(x_n)\}, \quad (2.10)$$

where x_i is the spacetime four-vector (t_i, \mathbf{x}_i) . This is now manifestly invariant with the exception of the details of the time-ordering which we will return to shortly. To manipulate four-vectors such as x_i we will use the mostly-minus convention for the Minkowski metric with $g_{00} = -g_{ii} = 1$ for $i = 1, 2, 3$.

2.2 Constructing the scalar field

Having obtained a Lorentz invariant S-matrix, we turn to the details of constructing the Hamiltonian density which lays the foundation for QFT. As opposed to quantum mechanics, QFT must incorporate a framework for producing and destroying particles. To this effort we define the creation operator $a^\dagger(q)$ which adds a particle with properties q to a state as [3]

$$a^\dagger(q) |\psi_{q_1 \dots q_n}\rangle \equiv |\psi_{q, q_1 \dots q_n}\rangle, \quad |\psi_{q_1 \dots q_n}\rangle = a^\dagger(q_1) a^\dagger(q_2) \dots a^\dagger(q_n) |0\rangle, \quad (2.11)$$

where $|\psi_{q_1 \dots q_n}\rangle$ is a multiparticle state and $|0\rangle$ is the vacuum state. The label q is a shorthand for all possible properties of the particle such as momentum, spin, and particle species. It can be shown that the creation operator's adjoint $a(q)$ removes a particle with properties q from a state and is hence known as the annihilation operator. In particular, we note that the action of the annihilation operator on the vacuum state is to return 0

$$a(q) |0\rangle = 0. \quad (2.12)$$

The operators $a^\dagger(q)$ and $a(q)$ are of fundamental importance due to the profound theorem that any operator can be expressed as a sum of products of creation and annihilation operators [3]. Motivated by this theorem we define the annihilation and creation fields for a spin-0 (scalar) particle [4]

$$\phi^+(x) \equiv \int d^3p u(x, \mathbf{p}) a(\mathbf{p}), \quad \phi^-(x) \equiv \int d^3p v(x, \mathbf{p}) a^\dagger(\mathbf{p}), \quad (2.13)$$

where the q label has been replaced with the 3-momentum \mathbf{p} and we consider only a single particle species with the implicit label n . By the above theorem we take the Hamiltonian density to be a polynomial in these fields

$$\mathcal{H}(x) = \sum_{NM} g_{NM} (\phi^-(x))^N (\phi^+(x))^M, \quad (2.14)$$

where g_{NM} are arbitrary coefficients. To obtain the full form of $\mathcal{H}(x)$ we need to determine the functions $u(x, \mathbf{p})$ and $v(x, \mathbf{p})$ in Eq. 2.13, as well as consider the restrictions on our polynomial in Eq. 2.14. We can do this through the constraints on the Hamiltonian density, the first of which is that $\mathcal{H}(x)$ must transform like a scalar field under a Lorentz boost or a space-time translation [3]. By going through the details of this condition, we arrive at the result

$$u(x, \mathbf{p}) = \frac{1}{(2\pi)^{3/2} \sqrt{2p^0}} e^{-ip \cdot x}, \quad v(x, \mathbf{p}) = \frac{1}{(2\pi)^{3/2} \sqrt{2p^0}} e^{ip \cdot x}, \quad (2.15)$$

where $p^0 = \sqrt{|\vec{p}|^2 + m^2}$ is the 0th component of the four-momentum of an on-shell particle with mass m . The second constraint is related to the details of time-ordering in Eq. 2.10 that we brushed over earlier. Since there is no decisive time-ordering for space-like separated points, we must require [3]

$$[\mathcal{H}(x_1), \mathcal{H}(x_2)] = 0 \text{ if } (x_1 - x_2)^2 \leq 0, \quad (2.16)$$

to obtain a Lorentz invariant S-matrix. This requirement makes it impossible to form $\mathcal{H}(x)$ as a product of $\phi^+(x)$ and $\phi^-(x)$ as we wrote in Eq. 2.14. We instead find that we must build $\mathcal{H}(x)$ as a polynomial in the field

$$\phi(x) \equiv \phi^+(x) + \phi^-(x), \quad \mathcal{H}(x) = \sum_N g_N (\phi(x))^N, \quad (2.17)$$

for arbitrary coefficients g_N . We have thereby constructed the unique scalar field

$$\phi(x) = \int \frac{d^3p}{(2\pi)^{3/2} \sqrt{2p^0}} (e^{-ip \cdot x} a(\mathbf{p}) + e^{ip \cdot x} a^\dagger(\mathbf{p})), \quad (2.18)$$

which will play a key role in establishing the Feynman rules.

2.3 Including charge

We have now seen how the form of the scalar field can be fixed by requiring Lorentz invariance of the S-matrix. However, the field we have constructed is for needlessly uninteresting particles with zero spin and no other intrinsic properties except a well-defined mass. Let us now introduce charge. We define the corresponding charge operator Q on a zero-spin state ket as

$$Q |\psi(p, n)\rangle = q_n |\psi(p, n)\rangle, \quad (2.19)$$

where q_n is the charge of particle species n . Since charge is a conserved quantity, we require the charge operator to commute with the Hamiltonian density. How this requirement arises may be understood in analogy with classical mechanics where conserved quantities have a Poisson bracket with the Hamiltonian of zero if the quantity has no intrinsic time-dependence. An equivalent statement arises in quantum mechanics with Poisson brackets replaced by commutators. However, if we evaluate this commutator using the scalar field for a single particle species in Eq. 2.18, we find that it is not zero. The solution to this issue has a profound physical meaning. If we introduce a second particle species \bar{n} with identical properties to n except opposite charge and construct a field as [3]

$$\phi(x) \equiv \phi_n^+(x) + \phi_{\bar{n}}^-(x) = \int \frac{d^3p}{(2\pi)^{3/2} \sqrt{2p^0}} (e^{-ip \cdot x} a(\mathbf{p}, n) + e^{ip \cdot x} a^\dagger(\mathbf{p}, \bar{n})), \quad (2.20)$$

we now satisfy the required commutation relations. Our theory thereby necessitates the existence of antiparticles. The Hamiltonian density $\mathcal{H}(x)$ may then be formed as a polynomial in the field $\phi(x)$ and its adjoint $\phi^\dagger(x)$.

2.4 Massless spin-1 fields

We now establish some properties of massless spin-1 fields which may be motivated similarly to the scalar fields above. The simplest example of a massless spin-1 field is a photon, the field of which may be written as [4]

$$A_\mu(x) = \int \frac{d^3p}{(2\pi)^{3/2} \sqrt{2p^0}} \sum_{i=1}^2 (\varepsilon_\mu^i(\mathbf{p}) a(\mathbf{p}, i) e^{-ip \cdot x} + \varepsilon_\mu^{i*}(\mathbf{p}) a^\dagger(\mathbf{p}, i) e^{ip \cdot x}), \quad (2.21)$$

where we sum over the possible photon polarization states i , $\varepsilon_\mu^i(\mathbf{p})$ are known as the polarization vectors, and $*$ indicates the conjugate. These two polarization states are related whether the projection of the photon's spin onto its momentum is \hbar or $-\hbar$, a property known as helicity [2]. As there is direct correspondence between polarization states and helicity, we may equivalently write the states as ε_μ^σ where σ is the helicity. Photons are however not the massless spin-1 field we will be most concerned with. Rather, we will focus on gluons. The exact field theoretic description of the gluon is significantly more complicated than that of photons due to the matrix colour charge they carry. However, we will be looking at scenarios that involve only a single soft gluon coupled to a quark in which case gluons and photons are remarkably similar. By carrying out detailed analysis of the color matrices for this case, it is found that the only difference for our calculation of the soft function will be an additional factor of $C_F = 4/3$, known as the colour factor, which we will manually add [5] [6].

3 Feynman diagrams

Equipped with knowledge of the S-matrix and the fields of spin-0 and spin-1 particles, we are now in a position to introduce Feynman diagrams, an ingenious way of schematically representing the calculation of S-matrix elements. In this section we will motivate how Feynman diagrams arise from evaluating an element of the S-matrix and outline their associated rules. No attempt is made at a detailed derivation or comprehensive overview of these rules. Rather, we emphasize only the rules that will be essential to our calculation of the soft function.

3.1 Evaluating an S-matrix element

Using the form of the S-operator in Eq. 2.10, let us attempt to evaluate an element of the S-matrix

$$S_{\mathbf{p}'_1 n'_1; \mathbf{p}'_2 n'_2 \dots \mathbf{p}_1 n_1; \mathbf{p}_2 n_2} = \sum_{n=0}^{\infty} \frac{(-i)^n}{n!} \int_{-\infty}^{\infty} d^4x_1 \dots d^4x_n (\langle 0 | \dots a(\mathbf{p}'_2, n'_2) a(\mathbf{p}'_1, n'_1) \mathcal{T}\{\mathcal{H}(x_1) \dots \mathcal{H}(x_n)\} a^\dagger(\mathbf{p}_1, n_1) a^\dagger(\mathbf{p}_2, n_2) \dots | 0 \rangle), \quad (3.1)$$

where the initial state particles have unprimed properties \mathbf{p} and n and the final state particles have primed properties \mathbf{p}' and n' . Our strategy for evaluating this element will be to move all the annihilation operators to the right towards the vacuum state $|0\rangle$ by using commutators. By doing so, we eventually end up annihilating the vacuum state which returns 0 as per Eq. 2.12. For example, if we need to move an annihilation operator past a creation operator we may use [3]

$$a(\mathbf{p}, n) a^\dagger(\mathbf{p}', n') = [a(\mathbf{p}, n), a^\dagger(\mathbf{p}', n')] + a^\dagger(\mathbf{p}', n') a(\mathbf{p}, n), \quad (3.2)$$

hence in swapping the order of these two operators we have picked up a commutator that pairs them. By repeating this process, we eventually end up having paired all creation and annihilation operators, including those in the fields and the field adjoints from insertions of the Hamiltonian density $\mathcal{H}(x)$. Our final result for the S-matrix element will thereby be a sum of integrals of products of commutators that may be between any combination of annihilation operators, creation operators, fields, and field adjoints. The details of evaluating these commutators will be neglected, but for spin-0 particles they yield simple factors of $(2\pi)^{-3/2}$ and $(2p^0)^{-1/2}$ with the exception of the case where we pair a field with a field adjoint. In this case we obtain a factor [3]

$$i\Delta_F(x, y) = \frac{i}{(2\pi)^4} \int_{-\infty}^{\infty} d^4q \frac{e^{iq \cdot (x-y)}}{q^2 - m^2 + i\epsilon}, \quad (3.3)$$

where $\Delta_F(x, y)$ is the Feynman propagator, and ϵ is a positive infinitesimal that is taken to 0 at the end of the calculation. The four-vector q^μ is closely related to p^μ , and we will return to its exact meaning shortly. Doing a similar calculation for the propagator for a massless spin-1 field yields the result [4]

$$\Delta^{\mu\nu}(x, y) = \int d^4q \, i\Pi^{\mu\nu}(q) e^{iq \cdot (x-y)}, \quad (3.4)$$

where in the Feynman gauge we have

$$i\Pi^{\mu\nu}(q) = \frac{1}{(2\pi)^4} \frac{-ig^{\mu\nu}}{q^2 + i\epsilon}. \quad (3.5)$$

3.2 Diagrammatic representation

Let us now connect the formal evaluation of an S-matrix element with a pictorial representation. As discussed, evaluating such an element yields a sum of commutators which pair different terms. This sum corresponds to a number of Feynman diagrams that when summed give the total amplitude. In such a diagram, commutators are represented by lines and the order of perturbation n , as it appears in Eq. 3.1, is indicated by n vertices. As seen from Eq. 3.1, each vertex must carry a factor ig where g is the coupling constant which appears in $\mathcal{H}(x)$. We distinguish between external lines which indicate pairing of an annihilation/creation operator with a field/field adjoint, and internal lines which indicates a pairing of a field and a field adjoint. External lines are singly connected to a vertex, whereas internal lines run between two vertices. The rules for calculating the contributions of such lines to the S-matrix element are then simply equivalent to the results obtained from evaluating the different commutators for such pairings. For example, an internal line for a spin-0 field gives a factor of the scalar propagator in Eq. 3.3. In this work we will use the convention that time runs along the x-axis and that lines representing particles will have arrows pointing towards increasing time, whereas antiparticle arrows point backwards in time.

We now make an important distinction. The propagators above have been given in position space, however it is usually more convenient to work in momentum space. To do so, we simply evaluate the integrals over spacetime in Eq. 3.1 before evaluating the integrals over momentum as they appear in the propagators. This yields several delta functions that enforce momentum conservation at each vertex in a Feynman diagram. The q that appeared in the propagators is therefore constrained to

be the momentum that flows into a vertex to which the corresponding internal line is attached. The situation is complicated slightly if we have two internal lines between the same vertices, hence forming a loop. In this case the momentum will be unconstrained, the implications of which we will return to when we evaluate a loop diagram later. In momentum space the propagators simplify and the internal lines instead yield a factor of

$$\frac{i}{(2\pi)^4} \frac{1}{q^2 - m^2 + i\epsilon}, \quad (3.6)$$

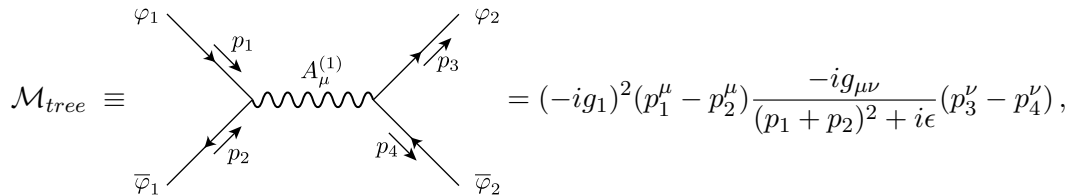
for spin-0 fields and a factor of $i\Pi^{\mu\nu}$ (Eq. 3.5) for spin-1 fields. In these equations there is an implicit integral over d^4q which simply constrains q as discussed above. However, if we have a loop and hence can not constrain q , this integral must be directly evaluated over infinite limits. We now briefly summarize the momentum space Feynman rules that will be relevant for our calculations which arise from careful evaluation of the relevant commutators [3] [4]:

1. Add a factor of $(2\pi)^{-3/2}(2p^0)^{-1/2}$ for every external line.
2. For an outgoing spin-1 particle, add a factor of the conjugate polarization vector $(\varepsilon_\mu^\sigma)^*$.
3. For an internal line, add a factor of the relevant propagator (Eq. 3.6 for a scalar field or 3.5 for a spin-1 field).
4. Add a factor of ig for every vertex. If the vertex is coupled to a spin-1 field, instead add $-ig$ times the sum of momenta aligned with the particle flow arrows minus the sum of momenta anti-aligned with the particle flow arrows.

We now have all the rules needed to derive the eikonal vertex, a crucial result for our upcoming calculation of the soft function.

3.3 The eikonal vertex

A very simple result arises when considering the Feynman diagram for a soft emission which we now derive. We will do this for the simple case of two scalar fields φ_1 and φ_2 which both interact with the spin-1 field $A_\mu^{(1)}$ and φ_2 additionally interacts with the spin-1 field $A_\mu^{(2)}$. This scenario may be taken as a proxy for the process in which an electron-positron pair annihilates to produce a quark-antiquark pair after which the (anti)quark radiates a gluon, with the obvious caveat that electrons and quarks are fermions whereas our fields are bosons. Let us first calculate the diagram with no emission of an $A_\mu^{(2)}$ particle by applying the above list of rules. We obtain, ignoring the factors of 2π and $2p^0$ for simplicity,



$$\mathcal{M}_{tree} \equiv \quad \quad \quad = (-ig_1)^2 (p_1^\mu - p_2^\mu) \frac{-ig_{\mu\nu}}{(p_1 + p_2)^2 + i\epsilon} (p_3^\nu - p_4^\nu),$$

where g_1 is the interaction strength for the coupling between $A_\mu^{(1)}$ and both the scalar fields. This expression may be simplified as

$$\mathcal{M}_{tree} = (-ig_1)^2 (-i) \frac{(p_1 - p_2) \cdot (p_3 - p_4)}{(p_1 + p_2)^2 + i\epsilon}. \quad (3.7)$$

Let us now calculate the same diagram, but this time with the emission of an $A_\mu^{(2)}$ particle from φ_2 . We then obtain

$$\mathcal{M} \equiv (-ig_1)^2 \frac{-i(p_1 - p_2) \cdot (p_3 + k - p_4)}{(p_1 + p_2)^2 + i\epsilon} \frac{i(-ig_2)(2p_3^\mu + k^\mu)}{(p_3 + k)^2 - m^2 + i\epsilon} (\varepsilon_\mu^\sigma)^*.$$

where g_2 is the interaction strength between $A_\mu^{(2)}$ and φ_2 . Consider now the scenario where the emission of the particle $A_\mu^{(2)}$ is soft such that $k \rightarrow 0$. This significantly simplifies our expression which becomes

$$\mathcal{M} = (-ig_1)^2 (-i) \frac{(p_1 - p_2) \cdot (p_3 - p_4)}{(p_1 + p_2)^2 + i\epsilon} \frac{g_2 p_3^\mu}{p_3 \cdot k + i\epsilon} (\varepsilon_\mu^\sigma)^*,$$

hence we have found something remarkable: the contribution from the soft emission factorizes from the result without any emission such that

$$\mathcal{M} = g_2 \frac{p_3 \cdot (\varepsilon^\sigma)^*}{p_3 \cdot k + i\epsilon} \mathcal{M}_{tree} \equiv g_2 \mathcal{E}_3^\mu(k) (\varepsilon_\mu^\sigma)^* \mathcal{M}_{tree}, \quad (3.8)$$

where $\mathcal{E}_i^\mu(k)$ is known as the eikonal vertex [7]. Whilst our derivation was carried out for a specific example, it turns out that this result generalizes to soft emissions from non-scalar fields [4]. In all generality, we write the eikonal vertex for an outgoing soft emission as

$$\mathcal{E}_i^\mu(k) = \pm \frac{p_i^\mu}{p_i \cdot k + i\epsilon}, \quad (3.9)$$

where the plus applies when the emitter is an outgoing particle and the minus applies when it is an outgoing antiparticle [4]. We are now equipped with all the Feynman rules needed for our calculation: the eikonal vertex, the massless spin-1 propagator, and the external line rules.

4 Thrust in SCET

Having acquired the relevant knowledge of Feynman diagrams, we now introduce the concepts that will set the stage for calculating the soft function for thrust.

4.1 Dijet production and thrust

A characteristic of high energy particles collisions is the formation of collimated sprays of particles known as jets [8]. Since evidence for the production of these was first observed at the Stanford Positron Electron Asymmetric Rings (SPEAR) in 1975 [9], jets have played a key role in the particle physics research effort. Like SPEAR, we will be considering electron-positron collisions, in particular the process

$$e^+ e^- \rightarrow q \bar{q} + X, \quad (4.1)$$

where X is any additional radiation from the quark q and the antiquark \bar{q} . We will consider the case where this is a dijet process by which is meant that only two back-to-back jets are formed, initiated by the quark and the antiquark. Alternatively stated, the radiation X is too soft or too collinear to the (anti)quark to qualify for forming a distinct third jet. One way of studying this process is through its thrust T defined as [10]

$$T = \max_{\vec{n}} \frac{\sum_i |\vec{p}_i \cdot \vec{n}|}{\sum_i |\vec{p}_i|}, \quad (4.2)$$

where the sum runs over all i final-state particles with \vec{p}_i being their respective 3-momenta and \vec{n} indicating any 3-vector with $|\vec{n}| = 1$. The 3-vector yielding the highest thrust is known as the thrust axis. This observable gives a quantitative measure of how the particles after a collision are distributed. In an event where the final-state particles are all either aligned or anti-aligned with the thrust axis, the thrust will be exactly 1. In a more general scenario we will have $T \approx 1$ if the radiation is overwhelmingly collinear to the (anti)quark and any non-collinear radiation is soft. In this case it is convenient to work with $\tau = 1 - T$ as $\tau \ll 1$ for $T \approx 1$. We thereby see a first hint at the motivation for applying SCET as the contribution to thrust will be dominated by soft and collinear particles for $\tau \ll 1$.

4.2 Factorization theorem for thrust

We now motivate an expression for τ that is valid for $\tau \ll 1$. In this regime, the thrust axis \vec{n} will be equivalent to the direction in which the (anti)quark moves. Motivated by this and letting \vec{n} be the direction of the quark, we define the four-vectors

$$n^\mu = (1, \vec{n}), \quad \bar{n}^\mu = (1, -\vec{n}), \quad (4.3)$$

where $-\vec{n}$ is the direction of the antiquark as the jets are back-to-back. Now consider dividing the final-state particles into two hemispheres depending on the sign of $\vec{p}_i \cdot \vec{n}$ such that one hemisphere contains the quark and the other contains the antiquark. The four-momenta p_1^μ and p_2^μ will be defined as the sum of the four-momenta in each hemisphere. By approximating the final-state particles to be massless such that the four-momentum of the (anti)quark may be expressed as

$$p_q^\mu = \frac{Q}{2} n^\mu, \quad p_{\bar{q}}^\mu = \frac{Q}{2} \bar{n}^\mu, \quad (4.4)$$

where Q is the center of mass energy of the collision, we may obtain the alternative expression [11]

$$\tau = \frac{p_1^2 + p_2^2}{Q^2}, \quad (4.5)$$

if $\tau \ll 1$. Since squaring a four-momentum yields a mass, this may also be interpreted as adding the masses of the jets in each hemisphere and rescaling by Q^2 . As discussed above, the contribution to τ in this regime will be dominated by soft and collinear particles. Let us therefore split the radiation in the quark hemisphere p_1^μ into p_{X_n} , the total four-momentum of radiation collinear to the quark (including the quark itself), and $p_{X_n^s}$, the soft radiation in this hemisphere. Similar quantities are defined for the antiquark, indicated by \bar{n} . By approximating to $\mathcal{O}(\tau)$ we obtain

$$Q^2 \tau = p_{X_n}^2 + p_{X_{\bar{n}}}^2 + Q[n \cdot p_{X_n^s} + \bar{n} \cdot p_{X_{\bar{n}}^s}], \quad (4.6)$$

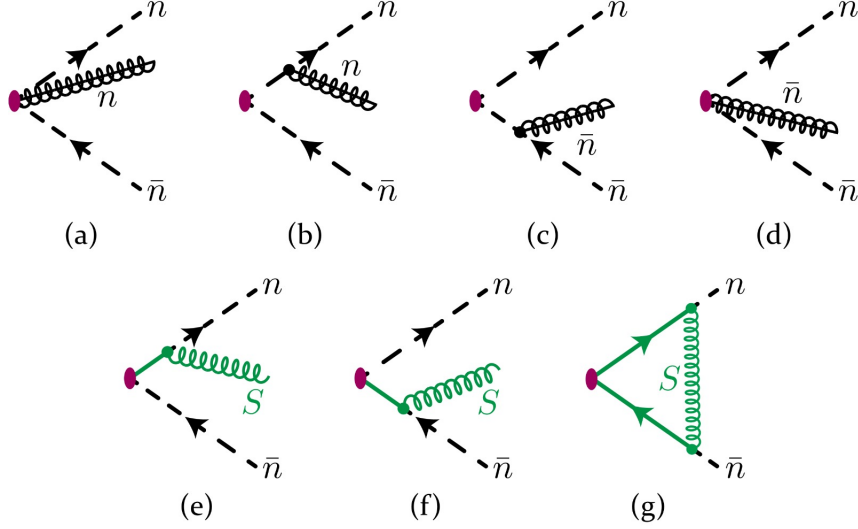


Figure 1: SCET Feynman diagrams for emission of a gluon from a quark-antiquark pair.

where we have explicitly separated the contributions from the radiation collinear to the quark, the radiation collinear to the antiquark, and the soft radiation. With this in mind we introduce the thrust factorization theorem as it may be derived in SCET. This gives the differential cross-section for thrust $\frac{d\sigma}{d\tau}$ for $\tau \ll 1$, normalized by the total cross-section σ_0 , as [4]

$$\frac{1}{\sigma_0} \frac{d\sigma}{d\tau} = H \int d(p_{X_n}^2) d(p_{X_{\bar{n}}}^2) d\ell J(p_{X_n}^2) J(p_{X_{\bar{n}}}^2) S_T(\ell) \delta\left(\tau - \frac{p_{X_n}^2 + p_{X_{\bar{n}}}^2 + Q\ell}{Q^2}\right), \quad (4.7)$$

where $\ell = n \cdot p_{X_n^s} + \bar{n} \cdot p_{X_{\bar{n}}^s}$. $J(p_{X_n}^2)$ and $J(p_{X_{\bar{n}}}^2)$ are known as the jet functions which describe how radiation collinear to the quark and antiquark respectively contribute to the cross-section. Similarly, $S_T(\ell)$ is the soft function for thrust which describes how the soft radiation contributes to the cross-section. This equation thereby succinctly formulates how contributions from the collinear and soft radiation factorize. The delta function enforces the measurement of τ to be in correspondence with Eq. 4.6. Finally, H is known as the hard function and describes the contributions to thrust that are from neither soft nor collinear radiation. This may seem contrary to our previous argument that in the regime $\tau \ll 1$, the only contribution will be from soft and collinear radiation. However, a virtual emission may very well be hard (highly energetic) if it is in a loop as its momentum is unconstrained. As illustrated by Eq. 4.7, a key point of SCET is that it treats particles of the same species differently depending on their momentum scale [12]. This will become more obvious upon consideration of Feynman diagrams as they appear in SCET which we will now discuss.

4.3 SCET Feynman diagrams

In accordance with the SCET thrust factorization theorem, the Feynman diagrams relevant for the $e^+e^- \rightarrow q\bar{q} + X$ process may be separated into those involving collinear radiation, soft radiation, and hard radiation. The collinear and soft diagrams are shown in Fig. 1 where we only consider gluon emission to first order. For simplicity, we do not show the diagrams for a hard or collinear

virtual emission. We have furthermore neglected showing the details of the electron-positron collision leading to the formation of the two quarks, and this is simply indicated by a red oval. The first four of these diagrams (a)-(d) represent the radiation of a real collinear gluon, represented by a black spring with a line through it. We distinguish between gluon emission collinear to the quark, the direction of which is indicated by n , and emission collinear to the antiquark with direction \bar{n} , see diagram (b) compared to (d). Furthermore, as seen by comparing diagrams (a) and (b), we distinguish between processes in which the gluon is emitted from the (anti)quark and those where the emission is from the background, indicated by the gluon originating from the red oval. More relevant to the calculation of the soft function are diagrams (e)-(g) which represent soft gluon emission, indicated by a green spring and the label S for soft. Diagrams (e) and (f) represent a real gluon emission, whereas diagram (g) represents a virtual gluon emission. We may wonder why a diagram in which the same (anti)quark emits and absorbs a virtual gluon is not included. Simply, the probability of such a process is zero if we consider a soft emission as may be seen by including two factors of the eikonal vertex (Eq. 3.9), once for each of the two vertices. This will yield a factor of either p_q^2 or $p_{\bar{q}}^2$ which is zero as the (anti)quark is approximated to be massless.

5 Calculating the soft function for thrust

We now set out to begin our calculation of the soft function for thrust. This will be sketched out in sufficient detail to gain an understanding of the main procedures and results, but the interested reader is referred to the appendix when relevant for the full details of how each step is carried out. We begin by defining the soft function in terms of our real and virtual matrix elements.

5.1 Setting up the calculation

As seen in Fig. 1, we have two diagrams with a real emission which will contribute to the soft function. Let us denote their summed matrix element as

$$\mathcal{M}_S^R(0 \rightarrow g_S; \{q\bar{q}\}) \equiv \text{diagram 1} + \text{diagram 2}, \quad (5.1)$$

where S and R stand for soft and real respectively and the arguments represent the emission of a soft gluon g_S from a quark-antiquark background. This notation highlights that we are considering a gluon emission sufficiently soft such that it leaves the (anti)quark four-momentum completely unaltered. We denote the corresponding real contribution to the soft function as $S_{T,R}^{[1]}(\ell)$ where R again stands for real and the superscript $[1]$ indicates that we are only considering the first order contribution. This is defined as

$$S_{T,R}^{[1]}(\ell) \equiv \int d^3k |\mathcal{M}_S^R(0 \rightarrow g_S; \{q\bar{q}\})|^2 \delta_S(\ell, k, n, \bar{n}), \quad (5.2)$$

where k is the gluon four-momentum. $|\mathcal{M}_S^R(0 \rightarrow g_S; \{q\bar{q}\})|^2$ gives the probability of a real soft gluon emission and $\delta_S(\ell, k, n, \bar{n})$ is a measurement function that imposes the relevant measurement

of thrust. By inspecting Eq. 4.6, the form $\delta_S(\ell, k, n, \bar{n})$ is easily determined. We require $\ell = n \cdot k$ if the gluon is in the quark hemisphere and $\ell = \bar{n} \cdot k$ if it is in the antiquark hemisphere. We hence write

$$\delta_S(\ell, k, n, \bar{n}) = \Theta_q(k)\delta(\ell - n \cdot k) + \Theta_{\bar{q}}(k)\delta(\ell - \bar{n} \cdot k), \quad (5.3)$$

where $\Theta_q(k)$ and $\Theta_{\bar{q}}(k)$ are the conditions for the gluon being in the quark or antiquark hemisphere respectively, the exact form of which we will return to shortly. Let us now consider the contribution from the virtual diagram to the soft function. Since there is no real emission, these will contribute to the cross-section at $\tau = 0$ hence our measurement function will be $\delta(\ell)$. By careful consideration of the virtual contribution we can show that the total soft function to first order gluon emission is

$$S_T^{[1]}(\ell) = \delta(\ell)(1 + 2 \text{Re}(\mathcal{M}_S^V)) + S_{T,R}^{[1]}(\ell), \quad (5.4)$$

where \mathcal{M}_S^V is the matrix element corresponding to diagram (g) in Fig. 1 and we have simply added the virtual and real contributions. Before moving on to the calculation of the real contribution, we briefly interlude to introduce light cone coordinates which will significantly simplify our calculation. Recall the definitions of n^μ and \bar{n}^μ given in Eq. 4.3 which indicate the directions that the quark and antiquark are travelling in. We seek to express any four-momentum k^μ using n^μ and \bar{n}^μ as basis vectors. This may be done by writing [12]

$$k^\mu = \frac{n^\mu}{2} \bar{n} \cdot k + \frac{\bar{n}^\mu}{2} n \cdot k + k_\perp^\mu, \quad (5.5)$$

where k_\perp^μ captures the components of k^μ perpendicular to n . To simplify this expansion we define

$$k^- \equiv \bar{n} \cdot k, \quad k^+ \equiv n \cdot k. \quad (5.6)$$

which are the variables we will use in our calculation.

5.2 Real contribution

Let us now calculate $S_{T,R}^{[1]}(\ell)$. As defined in Eq. 5.2, a key component of this is evaluating $|\mathcal{M}_S^R(0 \rightarrow g_S; \{q\bar{q}\})|^2$. It is now we benefit from the formula for the eikonal vertex in Eq. 3.9 derived earlier. Summing $g_i \mathcal{E}_i^\mu(\varepsilon_\mu^\sigma)^*$ over the two emitters (quark and antiquark), multiplying by the conjugate, and summing over helicities yields the squared matrix element

$$|\mathcal{M}_S^R(0 \rightarrow g_S; \{q\bar{q}\})|^2 = \frac{g^2}{(2\pi)^3 k^0} \frac{p_q \cdot p_{\bar{q}}}{(p_q \cdot k)(p_{\bar{q}} \cdot k)} = \frac{2g^2}{(2\pi)^3 k^0} \frac{1}{k^+ k^-}, \quad (5.7)$$

where we have converted to light cone coordinates using Eq. 5.5 and Eq. 4.4. To get the form of the measurement function, note that the conditions for the gluon being in the quark or the antiquark hemisphere are

$$\Theta_q(k) = \Theta(k^- - k^+), \quad \Theta_{\bar{q}}(k) = \Theta(k^+ - k^-), \quad (5.8)$$

respectively. This may be seen by expressing $\vec{k} \cdot \vec{n}$ in terms of k^+ and k^- , requiring $\vec{k} \cdot \vec{n} > 0$ for the quark hemisphere and oppositely for the antiquark hemisphere. We now have the full form of

the measurement function as defined in Eq. 5.3. Combining these this with the derived squared matrix element yields the integral for the real part of the soft function by using Eq. 5.2 as

$$S_{T,R}^{[1]}(\ell) = \frac{2g^2}{(2\pi)^3 k^0} \int d^3k \frac{1}{k^+ k^-} [\Theta(k^- - k^+) \delta(\ell - k^+) + \Theta(k^+ - k^-) \delta(\ell - k^-)] . \quad (5.9)$$

Computing this integral involves converting the integration measure to d^4k and carrying out the integral over the k_\perp component, the details of which may be found in Appendix A.1. Importantly, in the process of this we convert to calculating the cumulative soft function defined as

$$S_T^c(\ell^c) \equiv \int_0^{\ell^c} S_T(\ell) d\ell , \quad (5.10)$$

to simplify the integrals. We will stick to the cumulative soft function for the rest of the calculation. The final result from evaluating Eq. 5.9 is

$$S_{T,R}^c(\ell^c) = \frac{2\pi g^2}{(2\pi)^3} \left[\int_0^{\ell^c} \frac{dk^+}{k^+} \int_{k^+}^\infty \frac{dk^-}{k^-} + \int_0^{\ell^c} \frac{dk^-}{k^-} \int_{k^-}^\infty \frac{dk^+}{k^+} \right] , \quad (5.11)$$

from which it is clear that we have encountered an issue as all these integrals diverge. The integrals from k^\pm to ∞ diverge as $k^\pm \rightarrow \infty$, whereas the integrals from 0 to ℓ^c diverge as $k^\pm \rightarrow 0$. Such divergences are known as ultraviolet (UV) and infrared (IR) divergences respectively, and are commonly encountered in QFT calculations. More heuristically, IR divergences arise from the probability of emission of a soft particle going to infinity as its four-momentum goes to zero and oppositely, UV divergences arise from unconstrained momenta which can go to infinity.

We will now treat the UV divergence through dimensional regularization, a method commonly employed in QFT. The trick we seek to exploit is that the UV divergent integrals in Eq. 5.11 will converge if we have $(k^\pm)^{-1-\epsilon}$ in the integrand for some small $\epsilon > 0$. To this effort, we carry out the integral in $d = 4 - 2\epsilon$ dimensions instead of computing it in 4 dimensions. An integral over d^4k is then replaced by [4]

$$\int \frac{d^4k}{(2\pi)^4} \rightarrow \left(\frac{\mu^2 e^{\gamma_E}}{4\pi} \right)^\epsilon \int \frac{d^d k}{(2\pi)^d} , \quad (5.12)$$

where γ_E is Euler-Mascheroni constant and μ is known as the renormalization scale. At the end of a calculation ϵ is taken to 0 to restore the original 4 dimensions. Simultaneously, this will take all the added prefactors in Eq. 5.12 to 1, hence we are free to add them. The only crucial part of these prefactors is the renormalization scale μ which ensures that our expression preserves its dimensionality, hence μ must in this case have dimensions of mass. The other factors are simply added to obtain a convenient form for the final expansion of the soft function. If we carry out the integral for the soft function in Eq. 5.9 and compute in $4 - 2\epsilon$ dimensions instead of 4, converting to the cumulative soft function in the process, we obtain the result (see Appendix A.2)

$$S_{T,R}^c(\ell^c) = \frac{g^2}{4\pi^2} \frac{(\mu^2 e^{\gamma_E})^\epsilon}{\Gamma(1-\epsilon)} \left[\int_0^{\ell^c} \frac{dk^+}{(k^+)^{1+\epsilon}} \int_{k^+}^\infty \frac{dk^-}{(k^-)^{1+\epsilon}} + \int_0^{\ell^c} \frac{dk^-}{(k^-)^{1+\epsilon}} \int_{k^-}^\infty \frac{dk^+}{(k^+)^{1+\epsilon}} \right] , \quad (5.13)$$

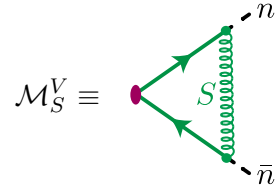
where Γ is the Gamma function. We have thereby successfully regularized the UV divergence as our integrals from k^\pm to ∞ go to 0 as $k^\pm \rightarrow \infty$ due to the extra ϵ in the power of the denominator. Evaluating the previously UV divergent integrals yields

$$S_{T,R}^c(\ell^c) = \frac{g^2}{4\pi^2} \frac{(\mu^2 e^{\gamma_E})^\epsilon}{\Gamma(1-\epsilon)} \frac{1}{\epsilon} \left[\int_0^{\ell^c} \frac{dk^+}{(k^+)^{1+2\epsilon}} + \int_0^{\ell^c} \frac{dk^-}{(k^-)^{1+2\epsilon}} \right], \quad (5.14)$$

for the real contribution to the cumulative soft function. We are left with only an IR divergence that we will now get rid of by including the virtual contribution.

5.3 Virtual contribution

As for the real contribution, the first step to calculating the virtual contribution is to evaluate the relevant matrix element. In this case we have two soft emission vertices so we include two factors of the eikonal vertex from Eq. 3.9. We also include the propagator for the internal gluon line from Eq. 3.5. Combining these pieces yields the matrix element



$$\mathcal{M}_S^V \equiv \text{diagram} = g^2 \int \frac{d^4 k}{(2\pi)^4} \frac{p_q^\mu}{p_q \cdot k + i\epsilon} \frac{-ig_{\mu\nu}}{k^2 + i\epsilon} \frac{p_{\bar{q}}^\nu}{p_{\bar{q}} \cdot k + i\epsilon}. \quad (5.15)$$

We will now drop the $i\epsilon$ in the eikonal vertex terms as they will not affect the integral. We then rewrite the matrix element as

$$\mathcal{M}_S^V = -g^2 \int \frac{d^4 k}{(2\pi)^4} \frac{i(p_q \cdot p_{\bar{q}})}{(p_q \cdot k)(p_{\bar{q}} \cdot k)(k^2 + i\epsilon)} = -2ig^2 \int \frac{d^4 k}{(2\pi)^4} \frac{1}{k^+ k^-} \frac{1}{k^2 + i\epsilon}, \quad (5.16)$$

where we have converted to light cone coordinates. When we considered how the real and virtual matrix elements are combined to give the soft function in Eq. 5.4, we found that the virtual contribution comes in the form $2\text{Re}(\mathcal{M}_S^V)$. Noting that $2\text{Re}(\mathcal{M}_S^V) = \mathcal{M}_S^V + (\mathcal{M}_S^V)^*$, it is clear that we must evaluate both \mathcal{M}_S^V and its conjugate. Converting the integral to d dimensions and making use of some standard identities (see appendix A.3), we obtain the result

$$2\text{Re}(\mathcal{M}_S^V) = -\frac{g^2}{4\pi^2} \frac{(\mu^2 e^{\gamma_E})^\epsilon}{\Gamma(1-\epsilon)} \frac{1}{\epsilon} \left[\int_0^\infty \frac{dk^+}{(k^+)^{1+2\epsilon}} + \int_0^\infty \frac{dk^-}{(k^-)^{1+2\epsilon}} \right]. \quad (5.17)$$

which looks remarkably similar to our result for the real contribution in Eq. 5.14. We may trivially convert to the cumulative soft function by integrating $\delta(\ell)2\text{Re}(\mathcal{M}_S^V)$ from 0 to ℓ^c which yields a simple factor of 1. To assemble the complete cumulative soft function, we have to add the contribution from $2\text{Re}(\mathcal{M}_S^V)$ to $S_{T,R}^c(\ell^c)$. In doing so we obtain terms like

$$\int_0^{\ell^c} \frac{dk^+}{(k^+)^{1+2\epsilon}} - \int_0^\infty \frac{dk^+}{(k^+)^{1+2\epsilon}} = - \int_{\ell^c}^\infty \frac{dk^+}{(k^+)^{1+2\epsilon}}, \quad (5.18)$$

hence it is clear that the inclusion of the virtual contribution has successfully cancelled the IR divergence as the lower limit of the integral is no longer 0. We are now in a position to obtain our final result.

5.4 Combining the pieces

To put our result into its standard form we introduce the strong coupling constant $\alpha_s = g^2/4\pi$ and manually add the colour factor $C_F = 4/3$ as discussed in section 2.4. We can then rewrite the contribution from the virtual diagram as

$$2 \operatorname{Re}(\mathcal{M}_S^V) = -\frac{\alpha_s C_F}{\pi} \frac{(\mu^2 e^{\gamma_E})^\epsilon}{\Gamma(1-\epsilon)} \frac{1}{\epsilon} \left[\int_0^\infty \frac{dk^+}{(k^+)^{1+2\epsilon}} + \int_0^\infty \frac{dk^-}{(k^-)^{1+2\epsilon}} \right], \quad (5.19)$$

and the contribution from the real diagrams from Eq. 5.14 as

$$S_{T,R}^c(\ell) = \frac{\alpha_s C_F}{\pi} \frac{(\mu^2 e^{\gamma_E})^\epsilon}{\Gamma(1-\epsilon)} \frac{1}{\epsilon} \left[\int_0^{\ell^c} \frac{dk^+}{(k^+)^{1+2\epsilon}} + \int_0^{\ell^c} \frac{dk^-}{(k^-)^{1+2\epsilon}} \right]. \quad (5.20)$$

When added, these two contributions yield IR-finite integrals as shown in Eq. 5.18 which may be simply evaluated to obtain the result

$$S_T^c(\ell^c) = 1 - \frac{\alpha_s C_F}{\pi} \frac{(e^{\gamma_E})^\epsilon}{\Gamma(1-\epsilon)} \frac{1}{\epsilon^2} \left(\frac{\mu^2}{\ell^c} \right)^{2\epsilon}, \quad (5.21)$$

where we have included the 1 from Eq. 5.4. By expanding this expression around $\epsilon = 0$ we obtain

$$S_T^c(\ell^c) = 1 + \frac{\alpha_s C_F}{\pi} \left[-\frac{1}{\epsilon^2} - \frac{2}{\epsilon} \ln \left(\frac{\mu}{\ell^c} \right) + \frac{\pi^2}{12} - 2 \ln^2 \left(\frac{\mu}{\ell^c} \right) \right] + \mathcal{O}(\alpha_s^2), \quad (5.22)$$

which is our final result for the cumulative soft function to $\mathcal{O}(\alpha_s)$. We may be alarmed by the factors of ϵ appearing in the denominator of the first two terms as we want to take $\epsilon \rightarrow 0$. However, these terms will cancel when we include the other components of the cross-section calculation, namely the jet functions and the hard function. This may be understood in analogy with classical electromagnetism where an electric potential may be infinite depending on the chosen reference point, but the electric field will always be finite as it is a measurable physical quantity. Similarly, the soft function is not a physical quantity, but the cross-section is. We furthermore see that employing our trick of dimensional regularization has left the soft function depending on the renormalization scale μ . Similarly to the ϵ divergences, this dependence will only drop out when we consider a physical quantity. Much more discussion of the rich physics behind renormalization may be had, however we will put this aside and instead outline some applications of soft functions to current research in precision collider physics.

6 Factorization and soft functions in current research

The study of jets has proven invaluable in furthering precision collider physics, allowing us to push the limits of precision measurements to new extremes. However, a significant obstacle to this research is the contamination that jets are plagued with. Such contamination has many sources, an example of which is pileup, the effect of secondary proton collisions occurring alongside the primary collision that is being measured [13]. To combat contamination, jet grooming techniques that aim to mitigate such have been under extensive study in recent years, in particular the soft drop grooming algorithm [14]. This groomer searches through the particle constituents of a jet, selectively removing soft wide-angle radiation. Recent research [15] has shown that applying the framework of SCET to

soft drop groomed jet observables yields factorization formulae similar to the one for thrust shown in Eq. 4.7. This finding has been immensely important as it has paved the way for furthering our theoretical understanding of groomed jets. Interest has thereby been sparked in calculating the soft functions for groomed observables, such as soft drop groomed jet radius [16], that appear in these factorization theorems. The process of such calculations takes a similar form to the steps outlined in this work, with additional complications from the constraints imposed by the groomer. In addition to contamination, non-perturbative effects such as hadronization corrections to jet observables provide another challenge to precision measurements. Due to the intrinsic difficulty in understanding hadronization from first principles, research is reliant on using hadronization models such as the cluster model [17] which are implemented in Monte Carlo event generators. However, such models have inherent uncertainties present which cannot be ascertained in a model-independent way. Progress has recently been made towards a model-independent understanding of such hadronization corrections. This was again achieved in the framework of factorization through SCET where a description of hadronization corrections to soft drop groomed jet mass was derived [18], thereby also necessitating further study of soft functions. However, despite progress, many unanswered questions remain. The quest for finding the optimal observables for making precision measurements is never-ending. Furthermore, whilst we were able to demonstrate cancellation of IR divergences in the soft function by including the virtual emission diagram, the non-existence of an IR-finite S-matrix remains a mathematical conundrum [19]. Research into the construction of a finite S-matrix is still ongoing [20], an achievement which would have a profound impact on not only precision collider physics, but all areas of theoretical particle physics.

7 Summary

This work sought to calculate the soft function for thrust, an important component in the factorization theorem for thrust derived in SCET that describes the contribution of soft radiation to the thrust cross-section. To achieve this, we began from the foundations of QFT, motivating the S-matrix from time-dependent perturbation theory and constructing the scalar field out of annihilation and creation operators. These two concepts proved crucial in understanding the origin of Feynman diagrams and their associated rules, allowing us to calculate the diagram for a soft emission. Since contributions to thrust are dominated by soft and collinear emissions in the regime where thrust is approximately one, the derived soft emission rule turned out to be essential. By applying it alongside other relevant Feynman rules, the matrix elements for real and virtual soft gluon emission at leading order were calculated. Combining these matrix elements with the relevant constraints allowed for the calculation of the thrust soft function, in the process of which both infrared and ultraviolet divergences appeared, serving as an insightful introduction to the different types of infinities that occur in QFT. By treating the ultraviolet divergence through dimensional regularization and cancelling the infrared divergence by including the virtual gluon emission diagram, the final result for the soft function was arrived at. The relevance of soft functions to current research in precision collider physics was discussed, the application of which may form the basis for further extension of this work.

References

- [1] C. W. Bauer, S. Fleming, D. Pirjol, and I. W. Stewart, “An effective field theory for collinear and soft gluons: Heavy to light decays,” *Physical Review D*, vol. 63, p. 114020, June 2001.
- [2] J. J. Sakurai and J. Napolitano, *Modern Quantum Mechanics*. Pearson, 2010.
- [3] S. Weinberg, *The Quantum Theory of Fields, Volume 1*. Cambridge University Press, 1995.
- [4] M. D. Schwartz, *Quantum Field Theory and the Standard Model*. Cambridge University Press, 2014.
- [5] A. Bassetto, M. Ciafaloni, and G. Marchesini, “Jet structure and infrared sensitive quantities in perturbative QCD,” , vol. 100, pp. 201–272, Nov. 1983.
- [6] M. E. Peskin and D. V. Schroeder, *An Introduction to Quantum Field Theory*. Perseus Book Publishing, 1995.
- [7] Z. Liu and P. Mao, “Infrared photons and asymptotic symmetries,” *Physics Letters B*, vol. 822, p. 136698, Nov. 2021.
- [8] R. Kogler, *Advances in Jet Substructure at the LHC: Algorithms, Measurements and Searches for New Physical Phenomena*. Springer, 2021.
- [9] G. Hanson *et al.*, “Evidence for jet structure in hadron production by e^+e^- annihilation,” *Phys. Rev. Lett.*, vol. 35, pp. 1609–1612, Dec 1975.
- [10] E. Farhi, “A QCD Test for Jets,” *Phys. Rev. Lett.*, vol. 39, pp. 1587–1588, 1977.
- [11] S. Catani, L. Trentadue, G. Turnock, and B. Webber, “Resummation of large logarithms in e^+e^- event shape distributions,” *Nuclear Physics B*, vol. 407, no. 1, pp. 3–42, 1993.
- [12] I. W. Stewart and C. W. Bauer, “Lecture notes on the soft-collinear effective theory,” 2014.
- [13] M. Aaboud *et al.*, “Identification and rejection of pile-up jets at high pseudorapidity with the ATLAS detector,” *Eur. Phys. J. C*, vol. 77, no. 9, p. 580, 2017.
- [14] A. J. Larkoski, S. Marzani, G. Soyez, and J. Thaler, “Soft Drop,” *JHEP*, vol. 05, p. 146, 2014.
- [15] C. Frye, A. J. Larkoski, M. D. Schwartz, and K. Yan, “Factorization for groomed jet substructure beyond the next-to-leading logarithm,” *JHEP*, vol. 07, 2016.
- [16] A. Pathak, I. W. Stewart, V. Vaidya, and L. Zoppi, “EFT for Soft Drop Double Differential Cross Section,” *JHEP*, vol. 04, p. 032, 2021.
- [17] B. Webber, “A QCD model for jet fragmentation including soft gluon interference,” *Nuclear Physics B*, vol. 238, no. 3, pp. 492–528, 1984.
- [18] A. H. Hoang, S. Mantry, A. Pathak, and I. W. Stewart, “Nonperturbative Corrections to Soft Drop Jet Mass,” *JHEP*, vol. 12, p. 002, 2019.

- [19] A. Strominger, “Lectures on the Infrared Structure of Gravity and Gauge Theory,” *arXiv e-prints*, p. arXiv:1703.05448, Mar. 2017.
- [20] H. Hannesdottir and M. D. Schwartz, “A Finite S -Matrix,” *arXiv e-prints*, p. arXiv:1906.03271, June 2019.

A Supplements for soft function calculation

A.1 Real contribution in 4 dimensions

We seek to evaluate the integral

$$S_{T,R}^{[1]}(\ell) = \frac{2g^2}{(2\pi)^3 k^0} \int d^3k \frac{1}{k^+ k^-} \delta_S, \quad (\text{A.1})$$

where we have abbreviated the measurement function $\delta_S(l, k, n, \bar{n})$ as δ_S . By using the identity [3]

$$\int \frac{d^3k}{2k^0} = \int d^4k \delta(k^2) \Theta(k^0), \quad (\text{A.2})$$

we can rewrite this as

$$S_{T,R}^{[1]}(\ell) = \frac{4g^2}{(2\pi)^3} \int d^4k \frac{\delta(k^2) \Theta(k^0)}{k^+ k^-} \delta_S. \quad (\text{A.3})$$

In light cone coordinates the integration measure is given by

$$d^4k = \frac{1}{2} dk^+ dk^- d^2k_\perp, \quad (\text{A.4})$$

and k^2 is given by [12]

$$k^2 = k^+ k^- + k_\perp^2 = k^+ k^- - \vec{k}_\perp^2. \quad (\text{A.5})$$

By applying these two equations we obtain

$$S_{T,R}^{[1]}(\ell) = \frac{2g^2}{(2\pi)^3} \int_0^\infty dk^+ \int_0^\infty dk^- \int d^2k_\perp \frac{\delta(k^+ k^- - \vec{k}_\perp^2)}{k^+ k^-} \delta_S, \quad (\text{A.6})$$

where the limits on the integrals over k^+ and k^- have been determined by considering the combined requirements of $k^+ k^- > 0$ from the delta function and $k^+ + k^- > 0$ from the theta function, noting that we can express k^0 as $(k^+ + k^-)/2$. Since d^2k_\perp is a standard area element, the integral over k_\perp may be evaluated as

$$\begin{aligned} \int d^2k_\perp \delta(k^+ k^- - \vec{k}_\perp^2) &= 2\pi \int dk_\perp k_\perp \delta(k^+ k^- - \vec{k}_\perp^2) \\ &= 2\pi \int dk_\perp \frac{k_\perp}{2\sqrt{k^+ k^-}} \delta(k_\perp - \sqrt{k^+ k^-}) = \pi, \end{aligned} \quad (\text{A.7})$$

hence

$$S_{T,R}^{[1]}(\ell) = \frac{2\pi g^2}{(2\pi)^3} \int_0^\infty \frac{dk^+ dk^-}{k^+ k^-} [\Theta(k^- - k^+) \delta(\ell - k^+) + \Theta(k^+ - k^-) \delta(\ell - k^-)], \quad (\text{A.8})$$

where we have now included the full form of the measurement function. We now switch to calculating the cumulative soft function

$$S_T^c(\ell^c) \equiv \int_0^{\ell^c} S_T(\ell) , \quad (\text{A.9})$$

to simplify this integral. We then obtain

$$\begin{aligned} S_{T,R}^c(\ell^c) &= \frac{2\pi g^2}{(2\pi)^3} \int_0^\infty \frac{dk^+ dk^-}{k^+ k^-} \int_0^{\ell^c} d\ell [\Theta(k^- - k^+) \delta(\ell - k^+) + \Theta(k^+ - k^-) \delta(\ell - k^-)] \\ &= \frac{2\pi g^2}{(2\pi)^3} \int_0^\infty \frac{dk^+ dk^-}{k^+ k^-} [\Theta(k^- - k^+) \Theta(\ell^c - k^+) + \Theta(k^+ - k^-) \Theta(\ell^c - k^-)] \\ &= \frac{2\pi g^2}{(2\pi)^3} \left[\int_0^{\ell^c} \frac{dk^+}{k^+} \int_{k^+}^\infty \frac{dk^-}{k^-} + \int_0^{\ell^c} \frac{dk^-}{k^-} \int_{k^-}^\infty \frac{dk^+}{k^+} \right] , \end{aligned} \quad (\text{A.10})$$

which is divergent.

A.2 Real contribution in d dimensions

We want to evaluate the integral

$$S_{T,R}^{[1]}(\ell) = \frac{2g^2}{(2\pi)^3 k^0} \int d^3 k \frac{1}{k^+ k^-} \delta_S = \frac{4g^2}{(2\pi)^3} \int d^4 k \frac{\delta(k^2) \Theta(k^0)}{k^+ k^-} \delta_S , \quad (\text{A.11})$$

by computing it in $d = 4 - 2\epsilon$ dimensions instead of 4 dimensions. To this effort we convert our integral to d dimensions as

$$S_{T,R}^c(\ell^c) \rightarrow \left(\frac{\mu^2 e^{\gamma_E}}{4\pi} \right)^\epsilon \frac{4g^2}{(2\pi)^{d-1}} \int_0^{\ell^c} d\ell \int \frac{d^d k}{k^+ k^-} \delta(k^2) \Theta(k^0) \delta_S , \quad (\text{A.12})$$

in accordance with Eq. 5.12 where we have also converted to calculating the cumulative soft function. Before trying to evaluate this, we will derive a useful identity that will make the integration trivial. To do so we need the generalized results [4]

$$d^{d-2} k_\perp = k_\perp^{d-3} dk_\perp d\Omega_{d-2} , \quad \Omega_d = \int d\Omega_d = \frac{2\pi^{d/2}}{\Gamma(d/2)} , \quad (\text{A.13})$$

where $\int d\Omega_d$ is the angular integral in d dimension and Γ is the Gamma function. We then see that

$$\begin{aligned} \int d^d k \delta(k^2) \Theta(k^0) &= \frac{1}{2} \int dk^+ dk^- d^{d-2} k_\perp \delta(k^2) \Theta(k^0) \\ &= \frac{1}{2} \Omega_{d-2} \int dk^+ dk^- dk_\perp k_\perp^{d-3} \delta(k^+ k^- - \vec{k}_\perp^2) \Theta(k^0) \\ &= \frac{1}{2} \Omega_{d-2} \int dk^+ dk^- dk_\perp \frac{k_\perp^{d-3}}{2\sqrt{k^+ k^-}} \delta(k_\perp - \sqrt{k^+ k^-}) \Theta(k^0) \\ &= \frac{1}{4} \Omega_{d-2} \int \frac{dk^+ dk^-}{(\sqrt{k^+ k^-})^{4-d}} \Theta(k^+) \Theta(k^-) \\ &= \frac{\pi^{1-\epsilon}}{2\Gamma(1-\epsilon)} \int \frac{dk^+ dk^-}{(k^+ k^-)^\epsilon} \Theta(k^+) \Theta(k^-) . \end{aligned} \quad (\text{A.14})$$

Computing the integral for the cumulative soft function in Eq. A.12 is now trivially done by using the above identity where we carried out the integral over k_\perp . We then obtain the result

$$S_{T,R}^c(\ell^c) = \left(\frac{\mu^2 e^{\gamma_E}}{4\pi} \right)^\epsilon \frac{2g^2}{(2\pi)^{d-1}} \frac{\pi^{1-\epsilon}}{\Gamma(1-\epsilon)} \int_0^{\ell^c} d\ell \int \frac{dk^+ dk^-}{(k^+ k^-)^{1+\epsilon}} \Theta(k^+) \Theta(k^-) \delta_S. \quad (\text{A.15})$$

Now include the measurement function, temporarily ignore the prefactors, and carry out the integral to obtain

$$\begin{aligned} S_{T,R}^c(\ell^c) &\propto \int_0^{\ell^c} d\ell \int \frac{dk^+ dk^-}{(k^+ k^-)^{1+\epsilon}} \Theta(k^+) \Theta(k^-) [\Theta(k^- - k^+) \delta(\ell - k^+) + \Theta(k^+ - k^-) \delta(\ell - k^-)] \\ &\propto \left[\int_0^{\ell^c} \frac{dk^+}{(k^+)^{1+\epsilon}} \int_{k^+}^\infty \frac{dk^-}{(k^-)^{1+\epsilon}} + \int_0^{\ell^c} \frac{dk^-}{(k^-)^{1+\epsilon}} \int_{k^-}^\infty \frac{dk^+}{(k^+)^{1+\epsilon}} \right]. \end{aligned} \quad (\text{A.16})$$

By including the prefactors we have our final result

$$S_{T,R}^c(\ell^c) = \frac{g^2}{4\pi^2} \frac{(\mu^2 e^{\gamma_E})^\epsilon}{\Gamma(1-\epsilon)} \left[\int_0^{\ell^c} \frac{dk^+}{(k^+)^{1+\epsilon}} \int_{k^+}^\infty \frac{dk^-}{(k^-)^{1+\epsilon}} + \int_0^{\ell^c} \frac{dk^-}{(k^-)^{1+\epsilon}} \int_{k^-}^\infty \frac{dk^+}{(k^+)^{1+\epsilon}} \right], \quad (\text{A.17})$$

hence we have successfully regularized the UV divergence.

A.3 Virtual contribution

To obtain the virtual contribution we must evaluate the integral

$$\mathcal{M}_S^V = -2ig^2 \int \frac{d^4 k}{(2\pi)^4} \frac{1}{k^+ k^-} \frac{1}{k^+ k^- - \vec{k}_\perp^2 + i\epsilon}. \quad (\text{A.18})$$

We seek to re-express this in $d = 4 - 2\epsilon$ dimensions. To avoid confusion with the ϵ in the denominator we relabel these as $\epsilon \rightarrow \xi$. We then have

$$\mathcal{M}_S^V = g^2 \left(\frac{\mu^2 e^{\gamma_E}}{4\pi} \right)^\epsilon (2\pi)^{-d} \Omega_{d-2} \int \frac{dk^+ dk^-}{k^+ k^-} \int dk_\perp \frac{-ik_\perp^{d-3}}{k^+ k^- - \vec{k}_\perp^2 + i\xi}, \quad (\text{A.19})$$

where Ω is the angular integral in $d - 2$ dimensions and we have used the expression for $d^{d-2} k_\perp$, both of which are defined in Eq. A.13. To evaluate the k_\perp integral it is useful to employ the identity [4]

$$\int dx \frac{x^a}{(x^2 + \Delta)^b} = \Delta^{\frac{a+1}{2}-b} \frac{\Gamma(\frac{a+1}{2}) \Gamma(b - \frac{a+1}{2})}{2\Gamma(b)}, \quad (\text{A.20})$$

for any x with a Euclidean measure. Taking $b = 1$, $a = d - 3$ and $\Delta = -k^+ k^- - i\xi$ we obtain

$$\int dk_\perp \frac{-ik_\perp^{d-3}}{k^+ k^- - \vec{k}_\perp^2 + i\xi} = i(-k^+ k^- - i\xi)^{-\epsilon} \frac{\Gamma(1-\epsilon) \Gamma(\epsilon)}{2}. \quad (\text{A.21})$$

Recall from our full form of the soft function in Eq. 5.4 that we need to evaluate $2 \text{Re}(\mathcal{M}_S^V)$. We therefore also need to compute the conjugate of the above result which is

$$-i(-k^+ k^- + i\xi)^{-\epsilon} \frac{\Gamma(1-\epsilon) \Gamma(\epsilon)}{2}. \quad (\text{A.22})$$

Let us now put together our results for \mathcal{M}_S^V and $(\mathcal{M}_S^V)^*$ to obtain

$$2 \operatorname{Re}(\mathcal{M}_S^V) \propto \int \frac{dk^+ dk^-}{k^+ k^-} [(-k^+ k^- - i\xi)^{-\epsilon} - (-k^+ k^- + i\xi)^{-\epsilon}]. \quad (\text{A.23})$$

To expand the $(-k^+ k^- \pm i\xi)^{-\epsilon}$ terms, we exponentiate them and make use of the complex logarithm. If $k^+ k^- > 0$ we obtain

$$\begin{aligned} e^{\ln(-k^+ k^- - i\xi)^{-\epsilon}} - e^{\ln(-k^+ k^- + i\xi)^{-\epsilon}} &= e^{-\epsilon[\ln(-k^+ k^-) - i\pi]} - e^{-\epsilon[\ln(-k^+ k^-) + i\pi]} \\ &= (k^+ k^-)^{-\epsilon} [e^{i\epsilon\pi} - e^{-i\epsilon\pi}] = 2i (k^+ k^-)^{-\epsilon} \sin(\pi\epsilon). \end{aligned} \quad (\text{A.24})$$

We note that this expansion gives zero if $k^+ k^- < 0$, hence the limits on the integrals over k^+ and k^- are fixed to both go from either 0 to ∞ or from $-\infty$ to 0. Since integrating over either of these limits will give the same result, we simply pick up a factor of 2 and choose the limits to be 0 to ∞ . By using the expression

$$\sin(\pi x) = \frac{\pi(1-x)}{\Gamma(x)\Gamma(1-x)}. \quad (\text{A.25})$$

and simplifying prefactors we obtain

$$2 \operatorname{Re}(\mathcal{M}_S^V) = -\frac{g^2}{4\pi^2} \frac{(\mu^2 e^{\gamma_E})^\epsilon}{\Gamma(1-\epsilon)} \int_0^\infty \frac{dk^+ dk^-}{(k^+ k^-)^{1+\epsilon}}. \quad (\text{A.26})$$

Noting that $\Theta(k^- - k^+) + \Theta(k^+ - k^-) = 1$, we can express this in a similar form to the real contribution

$$\begin{aligned} 2 \operatorname{Re}(\mathcal{M}_S^V) &\propto \int_0^\infty \frac{dk^+ dk^-}{(k^+ k^-)^{1+\epsilon}} [\Theta(k^- - k^+) + \Theta(k^+ - k^-)] \\ &\propto \int_0^\infty \frac{dk^+}{(k^+)^{1+\epsilon}} \int_{k^+}^\infty \frac{dk^-}{(k^-)^{1+\epsilon}} + \int_0^\infty \frac{dk^-}{(k^-)^{1+\epsilon}} \int_{k^-}^\infty \frac{dk^+}{(k^+)^{1+\epsilon}}, \end{aligned} \quad (\text{A.27})$$

so we finally obtain the expression

$$2 \operatorname{Re}(\mathcal{M}_S^V) = -\frac{g^2}{4\pi^2} \frac{(\mu^2 e^{\gamma_E})^\epsilon}{\Gamma(1-\epsilon)} \frac{1}{\epsilon} \left[\int_0^\infty \frac{dk^+}{(k^+)^{1+2\epsilon}} + \int_0^\infty \frac{dk^-}{(k^-)^{1+2\epsilon}} \right], \quad (\text{A.28})$$

for the virtual contribution to the soft function.